Supporting Information

Photo-crosslinked and photothermal *Flammulina velutipes* polysaccharide hydrogel loaded with caffeic acid-copper nanozyme for diabetic wound healing

Meimei Fu[‡,a], Qianru Xiang[‡,b,f], Zhuoyi Huang[‡,a,c], Wenjun Luo[a], Zhou Fang[a], Jintao Li[d], Yue Li[e], Zijun Xia[b], Yangjia Huang[b], Yitao Zhao[d], Wenzhen Liao[,b], Jinshan Guo[*,a,c]*

[a]Department of Histology and Embryology, NMPA Key Laboratory for Safety Evaluation of Cosmetics, School of Basic Medical Sciences, Southern Medical University, Guangzhou, 510515, P. R. China

[b]Department of Nutrition and Food Hygiene, Guangdong Provincial Key Laboratory of Tropical Disease Research, School of Public Health, Southern Medical University, Guangzhou, 510515, P. R. China

[c]CAS Key Laboratory of High-Performance Synthetic Rubber and its Composite Materials, Changchun Institute of Applied Chemistry, Chinese Academy of Sciences, 5625 Renmin Street, Changchun, 130022, P. R. China

[d]Department of Sports Medicine, Center for Orthopedic Surgery, Orthopedic Hospital of Guangdong Province, The Third School of Clinical Medicine, Guangdong

Provincial Key Laboratory of Bone and Joint Degeneration Diseases, The Third Affiliated Hospital of Southern Medical University, Guangzhou, 510630, P. R. China.

[e]Department of Plastic and Aesthetic Surgery, Nanfang Hospital of Southern Medical University, Guangzhou, 510515, P. R. China.

[f]Department of Clinical Nutrition, the Second School of Clinical Medicine, Zhujiang Hospital, Southern Medical University, Guangzhou, 510280, China.

‡These authors contribute equally.

*Corresponding authors:

Emails: jsguo4127@smu.edu.cn, guojinshan@ciac.ac.cn (Prof. J. Guo), wenzhenliao@163.com (Prof. W. Liao).

Figures

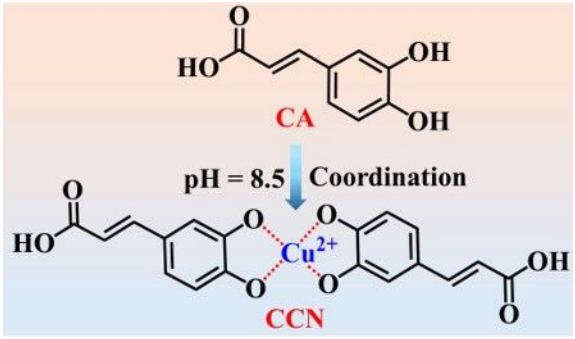

Figure S1. Schematic diagram of synthesis of CCN.

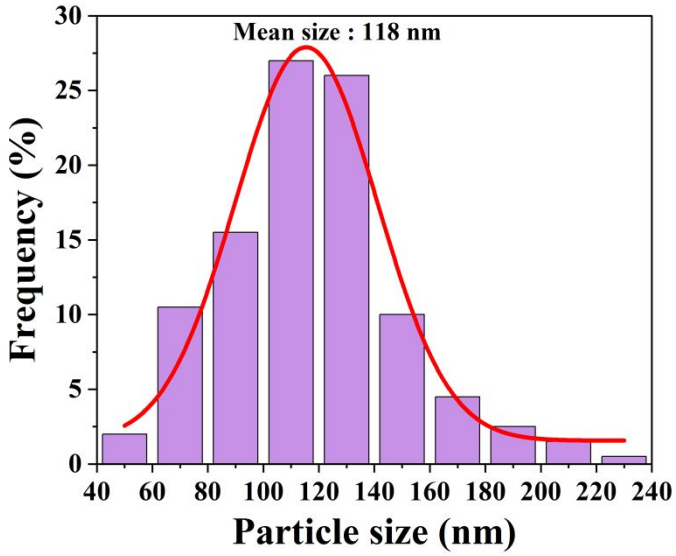

Figure S2. Particle size of CCN.

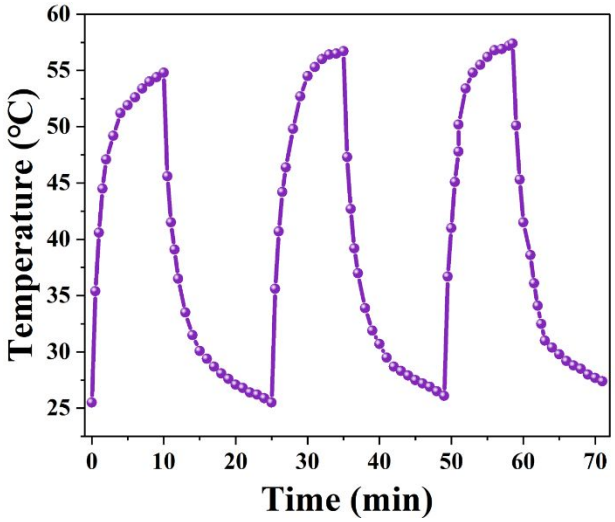

Figure S3. The temperature variation curve during four cycles of NIR irradiation on/off (power density = 2 W/cm^2).

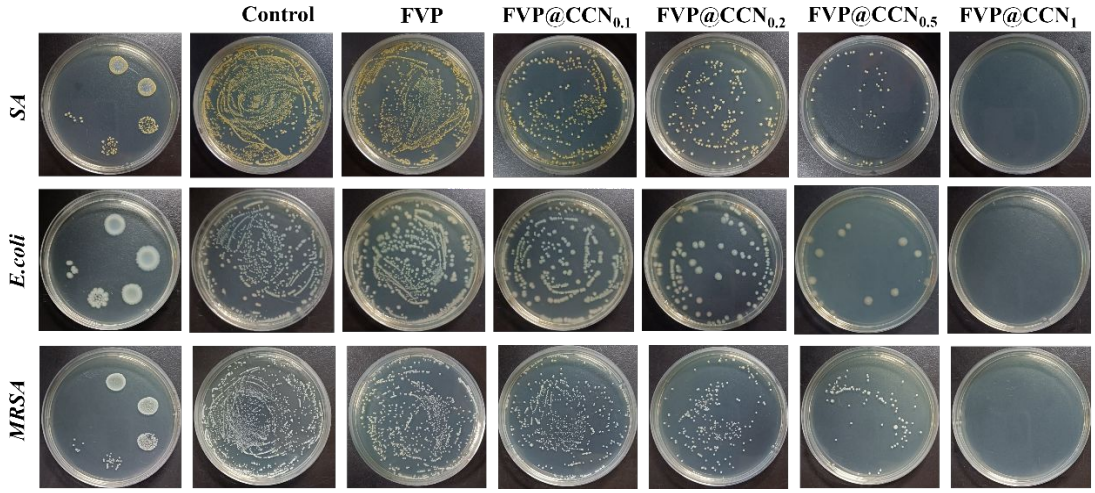

Figure S4. the macroscopic photos of survival bacterial colonies of *S. aureus, E. coli* and *MRSA* after exposed to FVP@CCN hydrogels.

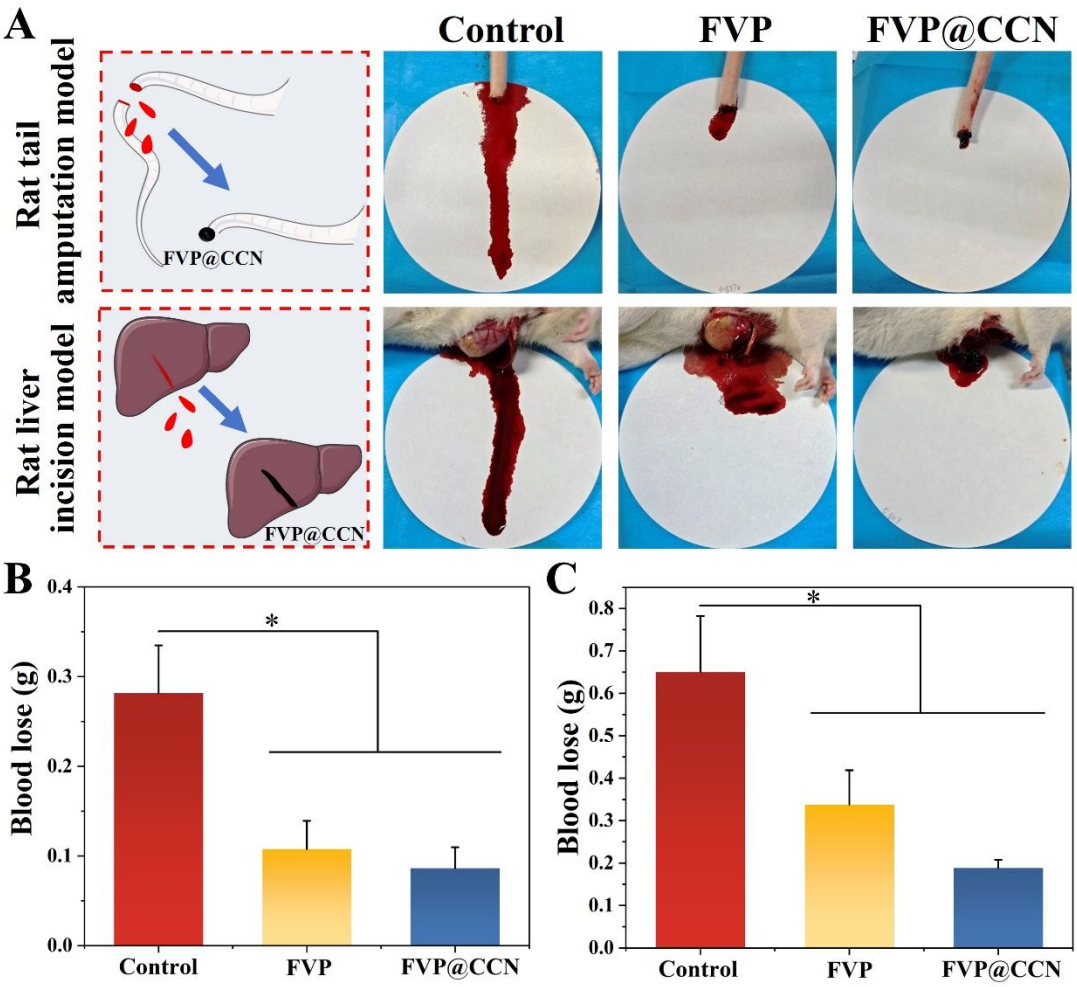

Figure S5. Hemostatic performance of FVP@CCN hydrogels. **A)** Schematic diagram and hemostatic photographs using rat tail amputation model and rat liver incision model. Quantification of blood loss in the **B)** tail amputation model and **C)** liver incision model across experimental groups (n = 3). *$p < 0.05$, **$p < 0.01$, ***$p < 0.001$

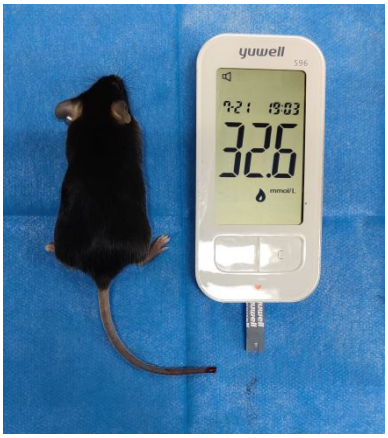

Figure S6. Determination of blood glucose in diabetic mice.

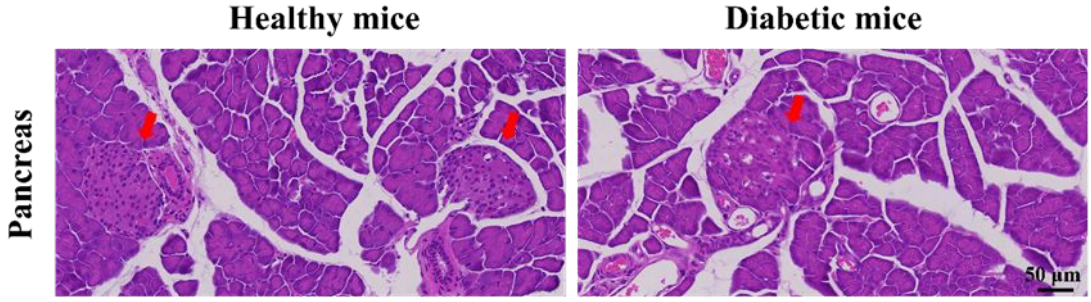

Figure S7. Representative H&E staining images of pancreas for healthy C57BL/6 mice and diabetic C57BL/6 mice.

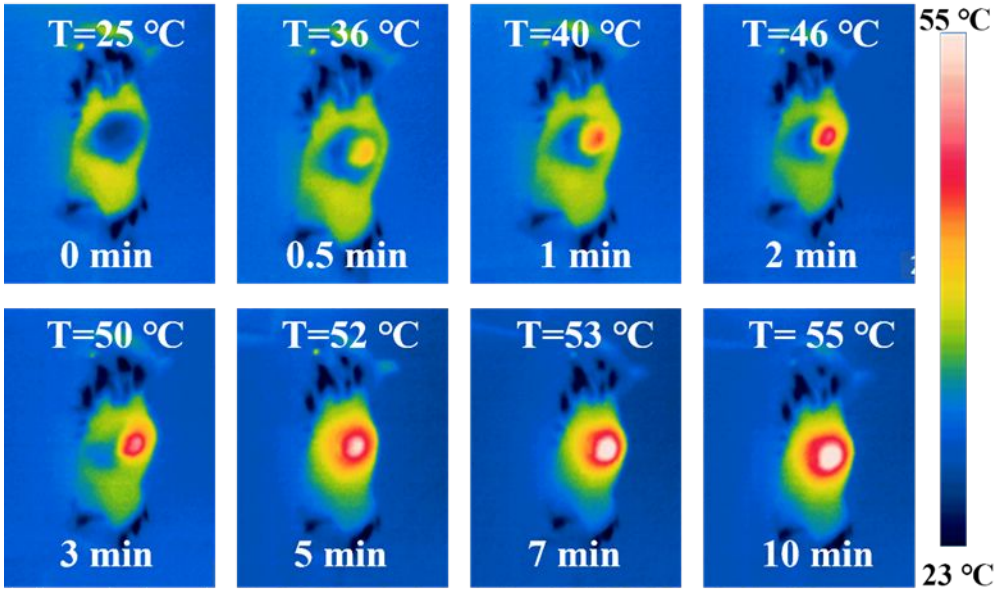

Figure S8. The photothermal temperature change images of diabetic wounds.

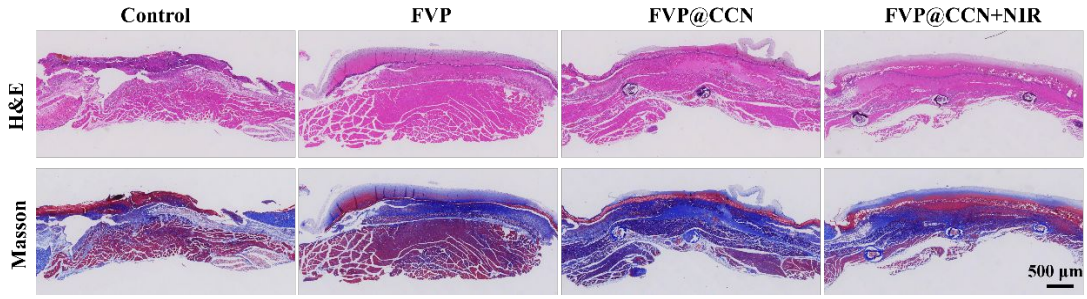

Figure S9. representative H&E staining and Masson staining images of treated skin tissues on the 3rd day post-surgery.

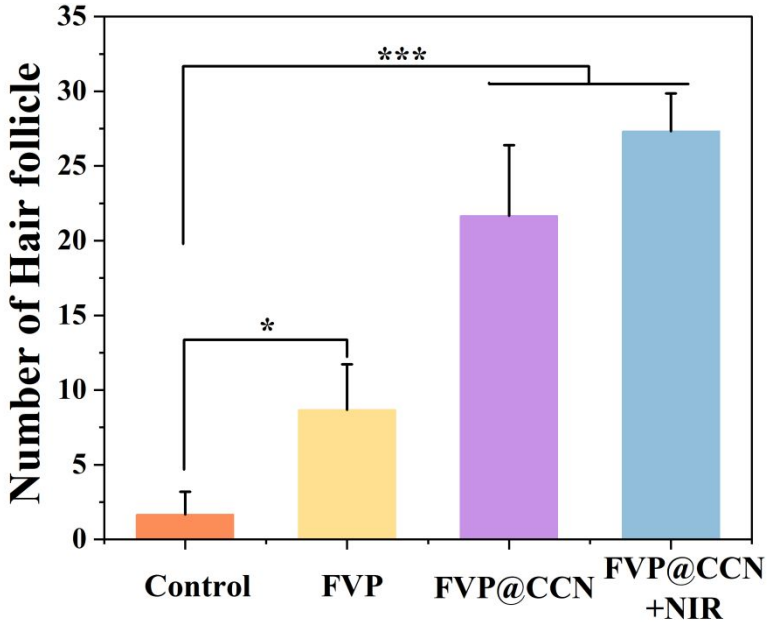

Figure S10. Number of hair follicles.

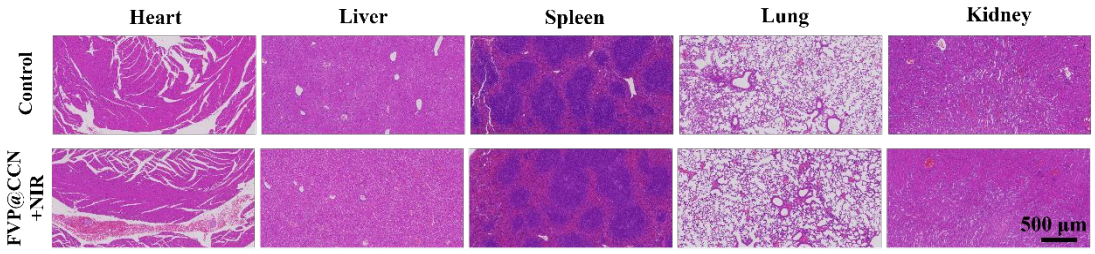

Figure S11. Biological safety of FVP@CCN hydrogels in vivo through H&E staining of heart, liver, spleen, lung, and kidney.

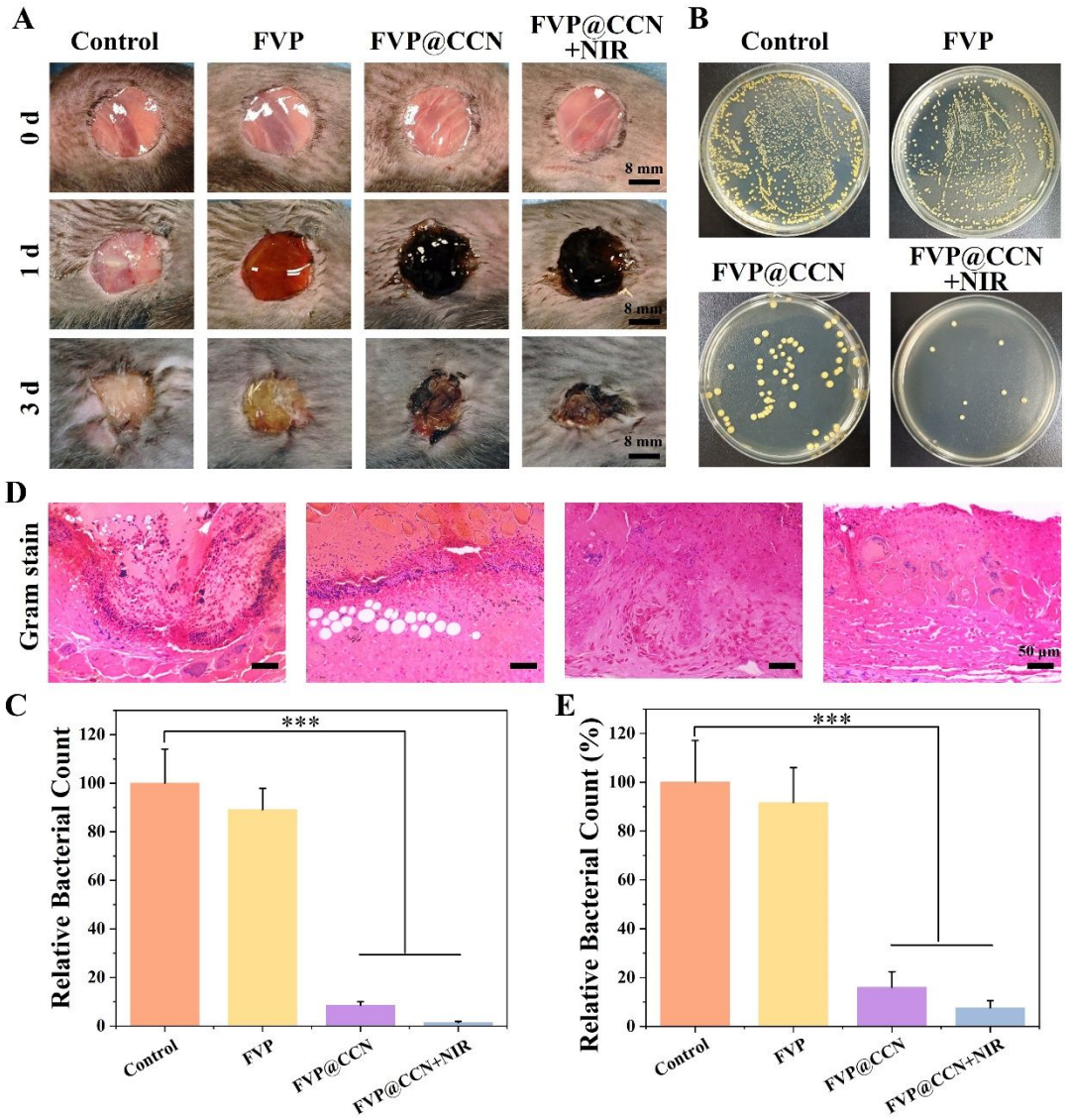

Figure S12. Antibacterial efficacy of FVP@CCN hydrogels in diabetic mouse wound infection models. **A)** Representative wound photographs of diabetic mouse across treatment groups (Control, FVP hydrogel, FVP@CCN hydrogel, and FVP@CCN+NIR) at indicated time points. **B)** Macroscopic wound morphology and **C)** quantitative analysis of *S. aureus* colony-forming units (CFUs) in infected wounds. **D)** Gram-stained histological sections of wound tissues on day 3 post-treatment and **E)** corresponding *S. aureus* CFU quantification (n = 3). *p < 0.05, **p < 0.01, ***p < 0.001.

Table S1

Carbohydrate and protein content of the crude polysaccharides and FVP

Name	Carbohydrate Mass Ratio (%)	Protein Mass Ratio (%)
Crude polysaccharides	77.36	11.09
FVP	98.57	0.00

Table S2

Chemical composition of FVP.

Name	Peak area	RT (min)	Mole Ratio (%)	Mass Ratio (μg/mg)
Fucose	24.61	4.89	7.51	58.99
Galactose	120.64	11.89	29.63	255.43
Glucose	249.55	12.84	41.28	355.94
Mannose	62.32	13.84	21.58	186.09